Neuron, Vol. 37, 513–523, February 6, 2003, Copyright ©2003 by Cell Press

Adaptive Coincidence Detection and Dynamic Gain Control in Visual Cortical Neurons In Vivo

Rony Azouz[1] and Charles M. Gray*
Center for Computational Biology and
Department of Cell Biology and Neuroscience
Montana State University
Bozeman, Montana 59717

Summary

Several theories have proposed a functional role for response synchronization in sensory perception. Critics of these theories have argued that selective synchronization is physiologically implausible when cortical networks operate at high levels of activity. Using intracellular recordings from visual cortex in vivo, in combination with numerical simulations, we find dynamic changes in spike threshold that reduce cellular sensitivity to slow depolarizations and concurrently increase the relative sensitivity to rapid depolarizations. Consistent with this, we find that spike activity and high-frequency fluctuations in membrane potential are closely correlated and that both are more tightly tuned for stimulus orientation than the mean membrane potential. These findings suggest that under high-input conditions the spike-generating mechanism adaptively enhances the sensitivity to synchronous inputs while simultaneously decreasing the sensitivity to temporally uncorrelated inputs.

Introduction

Several theories have proposed that figure-ground organization and attentional selection are signaled by the synchronization of distributed neuronal responses (Milner, 1974; von der Malsburg, 1981; Singer and Gray, 1995; Gray, 1999; Fries et al., 2001; Steinmetz et al., 2000). Critics of these theories have suggested, however, that selective synchronization is physiologically implausible when cortical networks operate at high levels of activity (Shadlen and Newsome, 1998; Shadlen and Movshon, 1999). It is argued that when cortical neurons operate in a "high-input regime," it becomes impossible for them to distinguish significant synchronous inputs from those that occur by chance. Consequently, states of selective synchronization are considered unlikely, and the precise temporal pattern of synaptic inputs is lost. In this framework, reliable sensory signals are thought to be conveyed by small populations of neurons on a time scale of tens of milliseconds, and neuronal synchrony having millisecond precision is considered functionally irrelevant (Shadlen and Newsome, 1998; Shadlen and Movshon, 1999).

Several lines of evidence contradict this argument. Principal among these is the widespread evidence for synchronous activity having millisecond precision. This form of activity has been observed in many cortical and subcortical areas, under a variety of behavioral conditions, and in a variety of species (Singer and Gray, 1995; Gray, 1994, 1999; Usrey and Reid, 1999). Thus, synchronous activity is not only plausible, but often surprisingly robust. A second line of evidence comes from studies of synaptic integration. Here it is well established that postsynaptic summation critically depends on the arrival times of presynaptic inputs to a cell (Alonso et al., 1996). Finally, multiple mechanisms intrinsic to cortical neurons can amplify the strength of synchronous inputs, thereby facilitating their propagation through the network (Schwindt and Crill, 1995; Stuart and Sakmann, 1995; Margulis and Tang, 1998; Destexhe and Pare, 1999; Azouz and Gray, 2000). In spite of this evidence, a significant conceptual problem remains for the temporal correlation models. It is not clear how neurons can discriminate real synchronous inputs from those that occur by chance during states of high network activity. One possibility is that an adaptive mechanism could act to simultaneously increase a cell's sensitivity to coherent synaptic input while decreasing the sensitivity to temporally unstructured synaptic input (von der Malsburg, 1981).

In a previous study, we have shown that the membrane currents underlying spike generation enhance synchronous excitatory inputs by lowering spike threshold in response to the transient depolarizations they evoke (Azouz and Gray, 2000; see also Henze and Buzsaki, 2001). Here, we extend this analysis to investigate the role of adaptive spike threshold on neuronal gain control and feature selectivity in cat striate cortex. We find two opposing effects of membrane potential (V_m) on action potential threshold. Slow depolarizations reduce overall cellular sensitivity and simultaneously increase the relative sensitivity to rapid depolarizations. This has the effect of dynamically increasing the sensitivity of cortical neurons to higher frequencies when they are depolarized. Consistent with this, we find that spike activity and high-frequency fluctuations in membrane potential are closely correlated and that both are more tightly tuned for stimulus orientation than the mean membrane potential. This suggests that the adaptive threshold mechanism amplifies transient depolarizations arising from synchronous synaptic inputs to shape the feature selectivity of cortical neurons. Together, these findings indicate that cortical neurons may overcome the constraints of the high-input regime by adaptively regulating their sensitivity to coincident synaptic inputs.

Results

The results of this study are based on recordings from 62 cells in cat striate cortex that had stable membrane potentials for durations of 20–90 min. Of these, 47 were visually stimulated with sine wave or square wave gratings, while 15 neurons were stimulated with drifting bars at intervals of 22.5° to determine their orientation tuning. Our goals were to determine the relations between spike

*Correspondence: cmgray@nervana.montana.edu
[1]Present address: Department of Physiology, Zlotowski Center for Neuroscience, Ben-Gurion University, Beer-Sheva 84105, Israel.

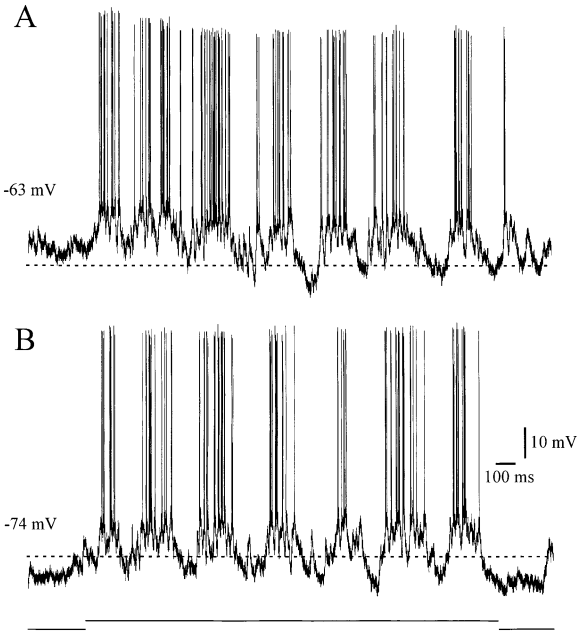

Figure 1. Cortical Neurons Exhibit Both Spontaneous and Stimulus-Dependent Changes in Membrane Potential (V_m) that Span a Broad Range of Amplitudes and Temporal Frequencies

The plots in (A) and (B) illustrate V_m fluctuations recorded from a cat striate neuron in response to two identical presentations of a drifting sine-wave grating. The dotted line in both plots illustrates the *baseline*-V_m, calculated by taking the average V_m across all trials during the first 250 ms of spontaneous activity in the session. The voltage values to the left of each plot indicate the average value of V_m on *each* trial calculated from the same period of spontaneous activity. These deviations from the *baseline*-V_m illustrate the slow spontaneous fluctuation in V_m that commonly occurs in all cortical neurons. Stimulus-evoked changes in V_m are superimposed on these slow fluctuations. They occur at the temporal frequency of the stimulus and at higher frequencies. Spike discharges occur during the depolarizing crests of these high-frequency fluctuations. The calibration bar at the bottom of the figure plots the time course of the stimulus.

threshold and variations in the magnitude and time course of V_m, and whether threshold variations influence the discharge properties and feature selectivity of cortical cells.

Dynamic Spike Threshold and Neuronal Gain Control

It is commonly observed that cortical neurons exhibit spontaneous variations in V_m that span 10–20mV in amplitude (Azouz and Gray, 1999). In the presence of such fluctuations (Figure 1), cortical neurons must dynamically compensate for the substantial variance in V_m if they are to convey accurate information about their sensory input. One likely candidate for such a function is the spike-generating mechanism, since it is well established that spike threshold varies as a function of the amplitude and time course of V_m (Hodgkin and Huxley, 1952a, 1952b; Noble, 1966; Fricker et al., 1999).

The extent to which this compensatory process operates in vivo is largely unknown, however. Therefore, to further understand the contribution of adaptive threshold on neuronal output, we performed several analyses. The first was to determine the influence of V_m on the voltage threshold at which spikes occur. For this, we calculated a prespike V_m ($\overline{V}_{m,ps}$) by taking the average subthreshold V_m during the 250 ms period preceding each spike (see Experimental Procedures) and compared this value to the voltage threshold measured for each corresponding spike. This and subsequent analyses were performed during the response to visual stimulation in order to assess the effects during sensory processing. The analysis revealed a significant linear correlation between $\overline{V}_{m,ps}$ and spike threshold for 92% (57/62) of the cells in the sample (Table 1), an example of which is shown in Figure 2A. The mean slope of the distributions was 0.49 $\pm$ 0.15, indicating on average that for each millivolt of membrane depolarization, spike threshold rises by about 0.5mV. Thus, by means of a simple and well-understood mechanism, spike threshold dynamically regulates cellular sensitivity by counteracting slow changes in V_m (Hodgkin and Huxley, 1952a, 1952b; Noble, 1966; Fricker et al., 1999).

These results suggest that cortical neurons tend to reduce their sensitivity by increasing spike threshold in response to inputs that lead to slow depolarizations. In contrast, recent evidence suggests that cortical neurons lower their threshold in response to rapid depolarizations (Azouz and Gray, 2000) and that this transient enhancement of sensitivity may increase as a function of the overall V_m (Carandini et al., 1996; Nowak et al., 1997). If this process operates in vivo, it could provide a mechanism for enhancing cellular responses to synchronous inputs. To test this hypothesis, we determined the relation between spike threshold and the rate of depolarization preceding each spike (dV_m/dt) and then evaluated the covariance between this relationship and the mean subthreshold V_m computed from the entire response period on each trial ($\overline{V}_{m,tm}$). An example of our findings is shown in Figure 2B, illustrating the relation between spike threshold and dV_m/dt for two trials having different $\overline{V}_{m,tm}$. On both trials, spike threshold showed an inverse, nonlinear dependence on dV_m/dt, but the relation was steeper, and the range of thresholds broader, when the cell was more depolarized. This effect could be due to changes in the distribution of dV_m/dt that covary with $\overline{V}_{m,tm}$ or to a change in the dependence of spike threshold on dV_m/dt as a function of $\overline{V}_{m,tm}$.

To test these two hypotheses, we first compared the range of dV_m/dt measured on each trial to the value of $\overline{V}_{m,tm}$ on the same trials. An example of the results is shown in Figure 2C. Although the range of dV_m/dt showed small variations across trials (σ = 0.1mV/ms), there was no dependence of this variable on $\overline{V}_{m,tm}$. Similarly, the range of spike thresholds showed no dependence on the range of dV_m/dt (data not shown). These results were consistent across a subsample of 25 cells. To test the second hypothesis, we fit the distribution relating dV_m/dt to threshold with a monoexponential function (Figure 2B) and then plotted the decay constant derived from the fit with respect to the value of $\overline{V}_{m,tm}$ recorded on the same trials (this analysis is permitted because the range of dV_m/dt does not vary across trials). The result, shown in Figure 2D, revealed an inverse linear dependence of the decay constant on $\overline{V}_{m,tm}$. We again applied this analysis to the same subsample of 25 cells and found the same relationship for each cell in the

Table 1. Linear Correlation Coefficients, and Their Corresponding Slopes, Calculated for the Dependence of Spike Threshold on $\bar{V}_{m,ps}$ and the Dependence of the Decay Constant on $\bar{V}_{m,tm}$

	$\bar{V}_{m,ps}$ versus Threshold	$\bar{V}_{m,tm}$ versus Decay Constant
Experimental data	$r = 0.83 \pm 0.29$, slope $= 0.49 \pm 0.15$ (n = 57 cells)	$r = 0.79 \pm 0.1$, slope $= -0.11 \pm 0.05$ (n = 25 cells)
H-H model—experiment (n = 18 trials)	$r = 0.62$, slope $= 0.41$	$r = 0.73$, slope $= -0.07$
H-H model—white noise (n = 20 trials)	$r = 0.66$, slope $= 0.42$	$r = 0.72$, slope $= -0.06$

Values are shown for the experimental data (mean ± SD), for the H-H model in response to currents derived from experimental data, and from bandpass white noise.

sample (Table 1). These findings demonstrate that although overall cellular sensitivity varies inversely with V_m, the relative sensitivity to rapid depolarization increases with V_m. This suggests that coincident synaptic inputs that lead to rapid depolarizations are likely to increase their relative effectiveness as a function of V_m.

To determine whether voltage-gated Na^+ and K^+ conductances underlie the two opposing effects of V_m on action potential threshold, we compared the behavior of a model neuron endowed with Hodgkin and Huxley (H-H)-like conductances to the behavior of the neuron in Figure 2. To do this, we first converted the V_m responses of the experimental data (spikes removed) to continuous records of current and then injected these currents into the model H-H neuron (see Experimental Procedures). We then applied the same analysis as shown in Figure 2 to the V_m responses of the model cell. These simulations revealed a significant linear correlation between $\bar{V}_{m,ps}$ and spike threshold, and between $\bar{V}_{m,tm}$ and the decay constant (Table 1).

The possibility exists, however, that because the injected currents were derived from experimental data, we may have introduced a rightward shift in the distribution of dV_m/dt in the simulated responses due to residual inward current preceding each spike. This in turn might have led to an artifactual increase in the dependence of spike threshold on dV_m/dt. To control for this possibility, we made two types of comparisons between our experimental data and the V_m responses of the H-H model. First, we calculated the cross-correlation coefficient between the experimental and simulated V_m measurements obtained from each trial of data after removal of all spikes. Second, we calculated the distribution of dV_m/dt preceding all simulated spikes and compared it to our experimental data. Both sets of measurements revealed that the experimental and simulated distributions were statistically indistinguishable. As a final control, we conducted an additional series of simulations by deriving currents from bandpass-filtered white noise having a frequency distribution similar to that observed

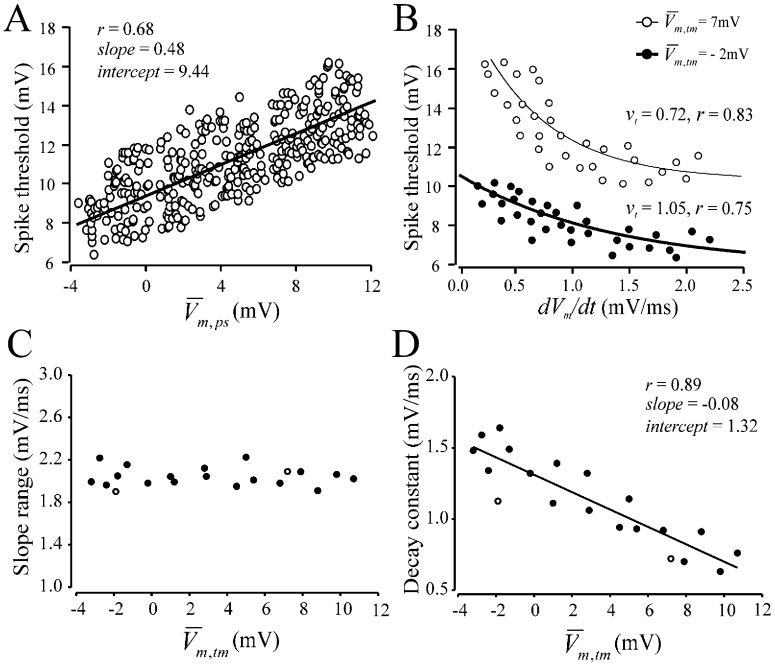

Figure 2. Dynamics of Voltage-Dependent Changes in Spike Threshold in a Striate Neuron

(A) Scatter plot of $\bar{V}_{m,ps}$ versus threshold for all visually evoked spikes recorded across trials. $\bar{V}_{m,ps}$ was taken as the average subthreshold V_m during the 250 ms period preceding each spike. The straight line depicts the linear fit to the data.

(B) Scatter plot of the rate of depolarization preceding a spike (dV_m/dt) versus spike threshold. The two curves illustrate data collected on two separate trials having a different value of $\bar{V}_{m,tm}$ The data were fit by the equation $Y = a + be^{-\dot{V}/v_t}$, where $\dot{V} = dV_m/dt$, and v_t is the decay constant in units of mV/ms. The closed and open symbols correspond to the separate trials.

(C) Scatter plot of the range of dV_m/dt measured on each trial versus $\bar{V}_{m,tm}$ on the same trials. The range of dV_m/dt values remains relatively constant across trials and shows no statistical dependence on $\bar{V}_{m,tm}$.

(D) Scatter plot of $\bar{V}_{m,tm}$ versus the decay constants computed from all trials in the session that were significantly fit by the equation in (B). The straight line shows the linear fit to the data. The open symbols correspond to the two trials depicted in (B). The value of $\bar{V}_{m,tm}$ in (B)–(D) was computed from the subthreshold activity during the entire period of visual stimulation.

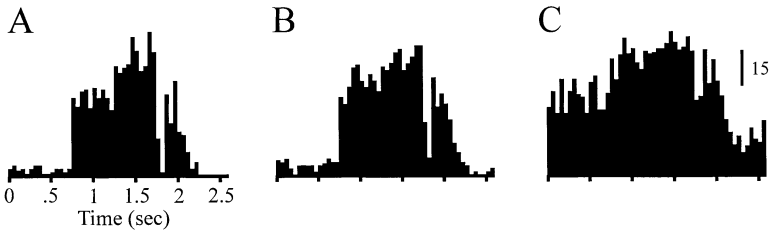

Figure 3. Adaptive Spike Threshold Regulates Discharge Characteristics

(A) PSTH computed from the responses of a regular spiking cell to 30 presentations of an optimally oriented, drifting sine wave grating (0.8 cycles/°, 2°/s, 10 cd/m²) presented to the contralateral eye.

(B and C) PSTHs computed from the spike responses of the H-H model neuron (B) and the I&F model neuron (C) following the injection of currents derived from the visual responses of the cell shown in (A). Note the similarity between the response of the H-H model and the experimental data, and the clear difference in the response of the I&F model.

experimentally. When we injected these currents into the model H-H neuron, we observed the same type of threshold dependence as reported for the experimental data (Table 1). Thus, our results confirm that the currents underlying action potential generation can largely account for the results described above and in Figure 2.

The Contribution of Dynamic Spike Threshold to Evoked Discharge Characteristics

Taken together, the preceding results have at least two important implications for the regulation of neuronal responses to sensory stimuli. First, they suggest that variations in spike threshold will alter cellular sensitivity to counteract slow changes in membrane potential. This could play an important role in reducing the impact of slow, stimulus-independent variations in V_m and in dynamically regulating the gain of neuronal responses to sensory stimuli. Second, they suggest that the relative sensitivity to rapid depolarizations will increase as a function of the mean level of depolarization. This could act to enhance the influence of fast fluctuations in V_m during high-input conditions by increasing the sensitivity of the spike-generating mechanism to coincident synaptic input.

We tested the first of these two predictions by comparing the behavior of two model neurons in response to currents derived from the experimental measurements of V_m during visual stimulation (see Experimental Procedures). Both neurons were modeled as a single compartment. One was endowed with H-H-like conductances, and the second was an otherwise identical integrate-and-fire (I&F) model. We used the spike activity from each model and the corresponding experimental data to compute the poststimulus-time histograms (PSTH) and then calculated the linear correlation coefficient between the experimental and simulated PSTHs (50 ms bin width). This provided a direct measure of the similarity between the responses of both models and the experimental data. As anticipated, the H-H model replicated the experimental data more accurately than the I&F model (Figure 3). The mean correlation coefficient between the experimental and H-H model PSTHs was 0.82 ± 0.15, while the mean coefficient computed between the experimental and I&F model PSTHs was 0.56 ± 0.31.

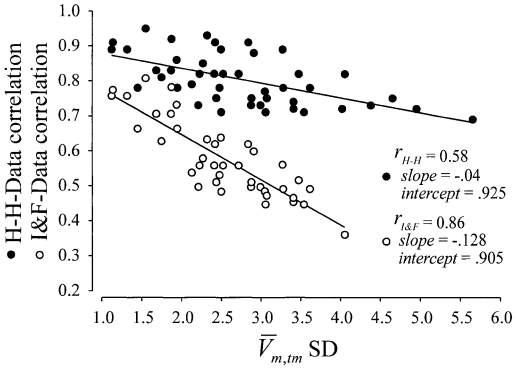

Figure 4. Hodgkin and Huxley Dynamics Predict the Behavior of Evoked Responses in Cortical Neurons

The graph shows a scatter plot of the correlation coefficients computed from the experimental and model PSTHs versus the standard deviation of $\overline{V}_{m,tm}$ (in mV) measured across trials from the experimental data (n = 47 cells). As the variance of $\overline{V}_{m,tm}$ increases, the H-H model maintains a close correlation with the experimental data while the I&F model diverges. The straight lines depict the linear fits to the data. Only statistically significant correlation coefficients are plotted.

We suspected that this difference was largely due to the inability of the I&F model to modify its spike threshold as a function of V_m. To test this idea, we plotted the correlation coefficients between the model and experimental PSTHs as a function of the standard deviation of $\overline{V}_{m,tm}$ measured *across trials* from the experimental data ($\overline{V}_{m,tm}$ corresponds to the average subthreshold V_m during the visual response on each trial). The correlation coefficients for the I&F model decreased sharply with the magnitude of $\overline{V}_{m,tm}$ variations, but the H-H model was much less perturbed by the same fluctuations (Figure 4). To determine if this difference was due to the influence of trial-to-trial variations in the DC level of V_m, we repeated the simulations after normalizing each trial to the *baseline*-V_m. This calculation (see Experimental Procedures) removes the DC component of the prestimulus V_m from each trial that deviates from the average prestimulus V_m measured across all trials. We then recalculated the correlation coefficients as before and found that this manipulation resulted in similar firing patterns between the experimental data and the model neurons for 92% of the cells in the sample ($r_{H\text{-}H}$ = 0.87 ± 0.15; $r_{I\&F}$ = 0.76 ± 0.31).

These results confirm our expectation that spike threshold acts as a dynamic gain control, enabling neurons to adjust their output sensitivity as a function of V_m. Figure 5 illustrates this effect experimentally in a cell that showed gradual hyperpolarization during the response to a high-contrast drifting grating (Carandini and Ferster, 1997). To determine the influence of threshold variations, we compared the discharge characteristics of the recorded cell to those observed in the two

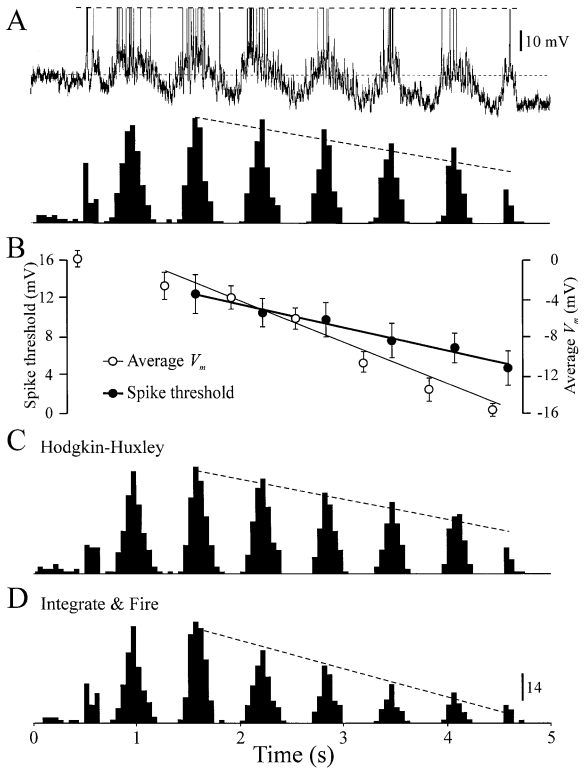

Figure 5. Adaptive Spike Threshold Counteracts Hyperpolarization Due to Contrast Adaptation

Data were collected from a regular spiking cell in response to an optimally oriented, drifting sine wave grating (0.7 cycles/°, 2°/s, 12 cd/m^2) presented to the contralateral eye.

(A) The upper trace shows the raw data collected on a single trial, and the lower trace shows the PSTH computed from the spike responses to 20 presentations of the stimulus. In the upper plot, spikes have been truncated, and the small dashed line shows the *baseline-V_m*.

(B) This graph plots the mean and standard deviation of the spike threshold (closed circles) and the average value of V_m (open circles) computed from a 100 ms epoch of data centered on the trough of the response to each cycle of the stimulus. The cell shows a gradual hyperpolarization that is accompanied by a corresponding drop in spike threshold. The first data point in the V_m plot is the *baseline-V_m* measured across trials.

(C) PSTH computed from the spike train of the H-H model.

(D) PSTH computed from the spike train of the I&F model. The dashed lines in the PSTH plots in (A), (C), and (D) show the linear regression to the peak firing rate on each cycle of the stimulus. Note the similarity of the PSTHs between the H-H model and the experimental data. Spike counts and thresholds were computed from a 450 ms window centered on the peak of each cycle of the response.

model neurons after injecting the currents derived from the experimental data. The covariance between the experimental and modeled cells was quantified by comparing the slope of the linear regression to the peak firing rate of each cycle of the stimulus (dashed lines in the PSTHs of Figures 5A, 5C, and 5D). The rate of adaptation displayed by the recorded cell (Figure 5A; slope = −40.8 spikes/s^2) was well approximated by the H-H model (Figure 5C; slope = −41.2 spikes/s^2), but less than that displayed by the I&F model (Figure 5D; slope = −47.8 spikes/s^2). This demonstrates that dynamic changes in spike threshold partially counteract the gradual hyperpolarization evoked by the stimulus and thereby adaptively adjust the cell's output (Figure 5B).

The Contribution of Dynamic Spike Threshold to Orientation Selectivity

Several studies have demonstrated that the orientation selectivity of synaptic inputs to striate neurons is broader than spike output (Nelson et al., 1994; Pei et al., 1994; Azouz et al., 1997; Volgushev et al., 2000; Carandini and Ferster, 2000; Anderson et al., 2000a). This has generally been interpreted as a "tip of the iceberg" effect, in which spikes are generated only in response to the most depolarized components of the V_m that cross a fixed firing threshold (Carandini and Ferster, 2000; Anderson et al., 2000a). However, our findings suggest a 2-fold dependence of spike threshold on V_m that could significantly affect the orientation selectivity of cortical neurons. First, changes in firing threshold will counteract slow changes in V_m, raising threshold during depolarization and lowering it during hyperpolarization. This negative feedback influence will tend to broaden orientation tuning by reducing cellular sensitivity at the preferred orientation and enhancing sensitivity at the null orientation. Second, fast variations in V_m will facilitate spike output, by lowering threshold during rapid depolarizations. Moreover, the magnitude of this influence will scale with the overall depolarization of the cell (Figure 2D), suggesting that the sensitivity to transient depolarization is greatest when cells are driven by strong depolarizing inputs. Given the evidence that γ band (30–80 Hz) oscillations in neuronal firing probability are well tuned for orientation (Gray and Singer, 1989; Gray et al., 1990; Anderson et al., 2000b), these findings suggest that high-frequency V_m fluctuations may make an important contribution to spike output in general and orientation selectivity in particular.

To test this conjecture, we compared the orientation selectivity of evoked spike count to $\overline{V}_{m,tm}$, spike threshold, and the integrated power of V_m in both low- (4–28 Hz) and high- (28–80 Hz) frequency bands. (All calculations performed on the subthreshold signals were done after removal of all action potentials [Azouz and Gray, 2000].) The results are shown for a single cell in Figure 6A. The orientation selectivity of the high-frequency fluctuations closely paralleled that of the spike output. Both of these signals were more selective than either $\overline{V}_{m,tm}$ or the low-frequency components of V_m (data not shown), while spike threshold showed a very broad, but detectable, selectivity. To quantify these relationships, we calculated the orientation bandwidth (2σ of the Gaussian fits to the tuning curves) for spike count, low- and high-frequency bands of V_m, and $\overline{V}_{m,tm}$ for a subsample of 15 cells. Scatter plots of this variable revealed that the spike count and high-frequency V_m fluctuations of each cell were more narrowly tuned than both $\overline{V}_{m,tm}$ and the low-frequency components of V_m (Figure 6B). Moreover, the orientation bandwidth of spike count and high-frequency power appeared to be systematically related. This observation was confirmed by calculating the linear correlation between these variables for all 15 cells. As shown in Figure 6C, the tuning bandwidths for spike count and the high-frequency components of V_m were

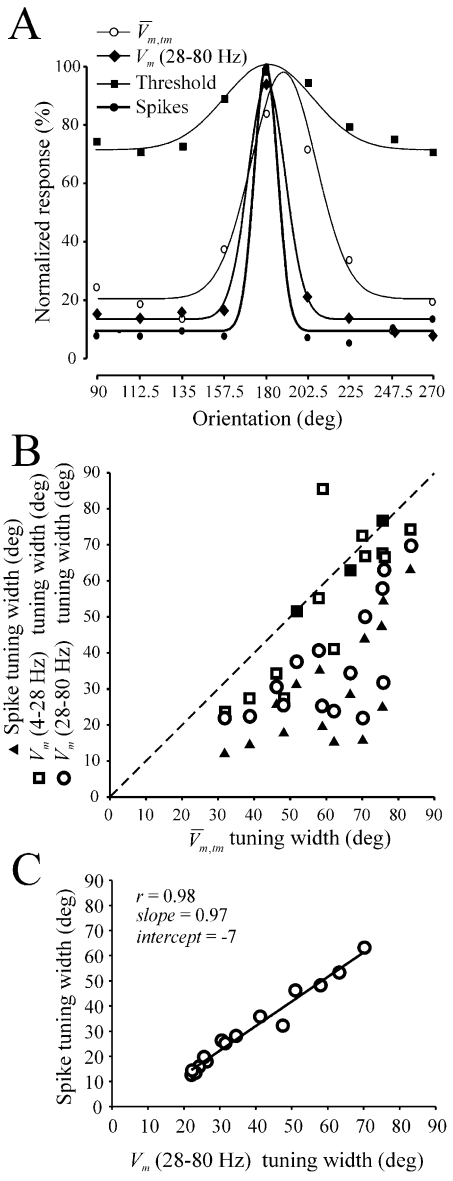

Figure 6. The Orientation Selectivity of Evoked Spikes Is Highly Correlated with the High-Frequency Components of V_m

(A) Normalized orientation tuning curves computed for $\overline{V}_{m,tm}$, high-frequency power, mean firing rate, and spike threshold from the evoked responses of a single cell.

(B) Scatter plot of the orientation tuning width (2σ of the Gaussian fit) of $\overline{V}_{m,tm}$ versus spike count, and the low- and high-frequency components of V_m for the sample of 15 cells. The tuning bandwidth of $\overline{V}_{m,tm}$ was similar to that of the low-frequency V_m components, and both were substantially broader than the high-frequency V_m components and the spike responses (mean bandwidth: $\overline{V}_{m,tm}$ = 61.1°; 4–28 Hz = 55.7°; 28–80 Hz = 38.1°; spikes = 30.2°). The closed squares represent values for which the Gaussian fit was not statistically significant.

(C) Scatter plot of the orientation tuning width of the high-frequency V_m components versus the spike responses for all 15 cells. The straight lines show the linear regression fit to the data.

tightly correlated ($p < 0.0001$). The same calculation applied to the low-frequency components of V_m was not statistically significant ($p = 0.0665$). These findings suggest that high-frequency fluctuations of V_m make a significant contribution to spike activity and hence orientation selectivity.

To further study the contribution of spike threshold to orientation selectivity, we compared the orientation tuning of both model neurons to the experimental tuning curves measured in the same 15 cells. As before, the model responses were measured by injecting the currents derived from the experimental tuning curves measured in the same cells (see Experimental Procedures). In each instance, the tuning width of the spike activity was narrower for the H-H model, and in 14 of the 15 cells, the tuning width of the H-H model responses was nearly identical to that of the experimental measurements (Figures 7A and 7B). These findings support the notion that adaptive threshold makes an important contribution to the orientation selectivity of cortical neurons.

As an additional test of this idea, we examined the influence of slow, stimulus-independent variations in V_m on the orientation selectivity of the two model neurons. We added a depolarizing DC component to the *response* phase of the injected current and determined the effect of varying the magnitude of this depolarization on the orientation tuning of the H-H and I&F model cells (Figure 7C). In both models, the depolarization led to higher firing rates at all orientations. However, the H-H model maintained its orientation selectivity across a broad range of depolarizing input, while the I&F model did not (Figure 7C). More importantly, as the magnitude of the depolarization increased, the tuning width of the I&F cell exceeded that of the underlying $\overline{V}_{m,tm}$ (dashed line in Figure 7C), while the H-H neuron dynamically regulated its output and maintained its selectivity. This finding demonstrates that the adaptive threshold mechanism preserves selectivity by decreasing cellular sensitivity to slow *stimulus-independent* V_m depolarizations (Figures 4 and 7C). When this effect is superimposed on γ band fluctuations in V_m that are tuned for orientation, it suggests that the two influences act synergistically to sharpen orientation tuning.

Discussion

Our results demonstrate a 2-fold dependence of spike threshold on V_m in cortical neurons recorded in vivo. During states of high network activity, dynamic changes in spike threshold reduce cellular sensitivity to slow depolarizations and concurrently increase the relative sensitivity to rapid depolarizations. This suggests that when cortical neurons are driven by strong input, their spike output will be preferentially determined by the amplitude of high-frequency components of the V_m. We tested this prediction by measuring the orientation selectivity of the mean and the high-frequency (γ band) components of the V_m. Our results showed a close correlation between spike activity and visually evoked high-frequency fluctuations in membrane potential. These findings suggest that the adaptive dynamics of spike generation act synergistically with input from the cortical network to shape the response properties of cortical neurons. Thus, rather than serving as a simple static nonlinearity, as assumed by many cortical models (Carandini and Ferster, 2000; Anderson et al., 2000a and references therein), the dynamics of spike threshold adaptively regulate response gain and the sensitivity to coincident synaptic inputs.

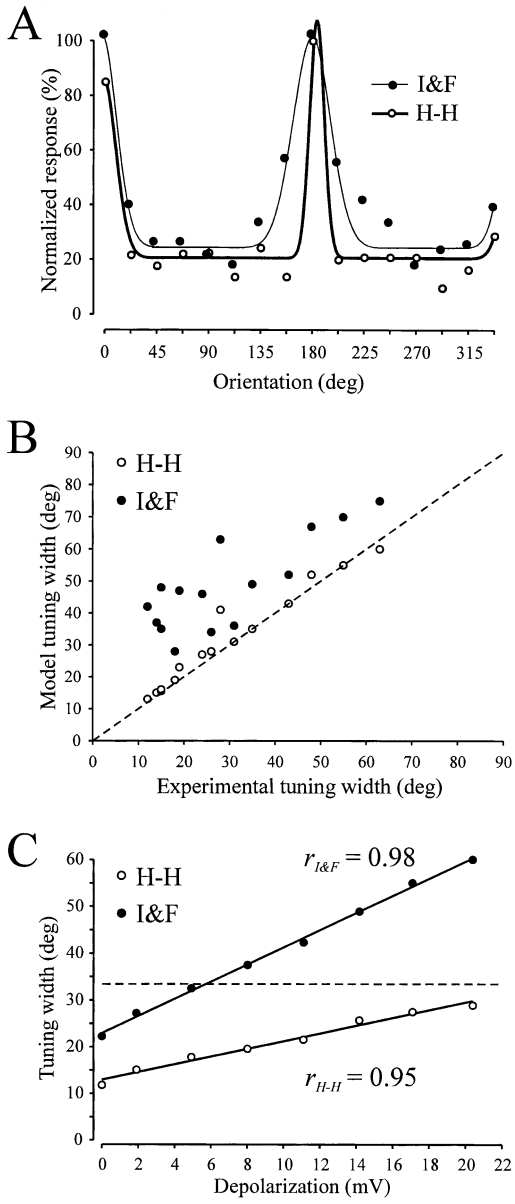

Figure 7. Hodgkin and Huxley Dynamics Contribute to the Feature Selectivity of Cortical Neurons

(A) This graph illustrates orientation-tuning curves for the spike output of the two model neurons measured under control conditions. (B) Scatter plot of the orientation tuning width of the experimental data versus the two model neurons spike responses. For all 15 cells tested, the tuning bandwidth of the I&F model was greater than that of the H-H model responses (data = 30.2°; H-H = 31.6°; I&F = 48.6°). (C) This graph illustrates the systematic dependence of orientation bandwidth as a function of added V_m depolarization. The straight lines show the linear fits to the data. The dashed line in (C) depicts the orientation bandwidth of the experimental $\overline{V}_{m,tm}$. Note that the orientation bandwidth of the H-H model is always below that of $\overline{V}_{m,tm}$, while that of the I&F model exceeds it at moderate levels of depolarization.

Methodological Considerations

Before discussing the underlying mechanisms and implications of these findings, it is important to consider the assumptions upon which our interpretations are based. The first concerns our definition of spike threshold. We have operationally defined threshold as the membrane voltage at the onset of spike upstroke (see Fricker et al., 1999; Anderson et al., 1987 for related measures). This was the only practical measure available to us, and we cannot exclude the possibility that it introduced some form of error in the estimate of threshold. Second, we generally assume that our impalements occur at or near the soma and that our measurements of V_m reflect the voltage fluctuations at the site of spike initiation. Again, we cannot confirm these assumptions. In spite of these uncertainties, however, the systematic agreement between our findings and the predicted dependence of spike initiation on V_m (Azouz and Gray, 2000; Hodgkin and Huxley, 1952a, 1952b; Noble, 1966; Fricker et al., 1999) suggest that our measure of spike threshold accurately reflects the spike initiation process (for further discussion, see Azouz and Gray, 2000).

Our conclusions also rest on the assumption that rapid depolarizations arise from synchronous synaptic inputs, while slow changes in V_m reflect sustained, independent inputs. While this interpretation is fully consistent with the properties of synaptic integration (Destexhe and Pare, 1999; Azouz and Gray, 2000), it neglects the role of dendrites in shaping the integration process. Dendritic integration may turn synchronous inputs into slow V_m variations at the soma if these inputs are spatially distributed. Alternatively, asynchronous synaptic inputs in different parts of the dendritic tree may yield rapid depolarizations at the soma, if they have the right magnitude and timing. While we cannot exclude the contribution of either of these processes, our interpretation provides the simplest explanation consistent with experimental and theoretical evidence (Usrey and Reid, 1999; Alonso et al., 1996; Azouz and Gray, 1999, 2000; Diesmann et al., 1999).

Another issue deserving mention is the surprisingly systematic correlation between the tuning bandwidth of the γ band component of V_m and spike activity (Figure 6C). This raises the concern that the magnitude of γ band activity may be linked to the occurrence of spikes and hence that the correlation may be a measurement artifact. In our analysis, we were careful to remove all spikes prior to calculating the γ band component. However, it is possible that voltage-gated currents occurring prior to each spike could have contributed to our measure (Gray and McCormick, 1996; Azouz and Gray, 2000). One test of this notion would be to measure the orientation bandwidth of the γ band component while the cells are held below firing threshold using DC current injection. Although such data is not available, several studies have reported that visually evoked γ band oscillations in V_m persist, and even increase in amplitude, when cells are held below firing threshold (Jagadeesh et al., 1992; Bringuier et al., 1996; Azouz and Gray, 2000). These data demonstrate that in many cells γ band activity is due to synaptic input and not directly or artifactually related to the occurrence of spike activity.

Finally, we interpret the change in relative sensitivity to rapid depolarization as a function of V_m as evidence of an adaptive bandpass mechanism. While this assumption is supported by our data, a quantitative analy-

sis would be required to fully address this issue (Carandini et al., 1996).

Cellular Mechanisms of Adaptive Threshold

Our findings can best be accounted for by the classical Hodgkin-Huxley theory, which describes the voltage- and time-dependent changes in sodium and potassium conductance (Hodgkin and Huxley, 1952a, 1952b; Noble, 1966; Fricker et al., 1999). In this model, spike threshold will rise when the percentage of available sodium and potassium channels falls and rises, respectively. The critical factor controlling the dynamics of this process is likely to be the differential kinetics of the voltage-dependent activation and inactivation of these channels. Slow depolarizations lasting hundreds of milliseconds, such as those evoked by visual stimuli, will activate both Na^+ and K^+ channels, while simultaneously inactivating the Na^+ channels. These effects will reduce Na^+ channel availability, increase K^+ channel availability, and thereby lead to an overall rise in spike threshold and a reduction of cellular sensitivity. Conversely, rapid depolarizations will lead to substantial Na^+ channel activation that precedes both the inactivation of Na^+ channels and the activation of K^+ channels. These events will cause a transient drop in spike threshold that results from a sudden increase in Na^+ channel availability.

Interestingly, we found that the relative reduction in spike threshold that occurs in response to rapid depolarizations was inversely proportional to the overall (i.e., mean) membrane potential. This suggests that during strong and sustained depolarizations, when Na^+ channel availability is relatively low, the remaining population of available Na^+ channels can be more readily activated by rapid depolarizations. We confirmed that this effect could also be accounted for by the voltage-gated Na^+ and K^+ channels by showing a similar relationship for the responses of the H-H model to injected currents derived from the visually evoked responses.

It should be pointed out, however, that additional factors are likely to contribute to the regulation of spike threshold. Other voltage-gated conductances, such as slow potassium currents with high activation potentials, could play a significant role in regulating spike threshold. Similarly, voltage-gated Na^+ channels are known to be modulated by a variety of neurotransmitters (Cantrell and Catterall, 2001; Carr et al., 2002), which can have effects on current magnitude, voltage-dependence, and gating kinetics. Each of these actions could have affected our results, particularly if the relevant neurotransmitters were released during the barrage of synaptic activation evoked by visual stimulation.

Functional Implications

Although the detailed cellular mechanisms underlying our results are beyond the scope of this study, the functional implications are relatively clear. When cells are hyperpolarized, spike threshold will fall to increase cellular sensitivity to depolarizations having a broad range of temporal frequencies. Conversely, when cells become depolarized, spike threshold will increase to reduce cellular sensitivity to further slow depolarizations while preserving, or even enhancing, the relative sensitivity to rapid depolarizations. This adaptive mechanism will have two predominant effects. One will be to act as a dynamic gain control to counteract changes in membrane potential and neuronal firing rate. This may contribute to response normalization and contrast gain control, enabling cortical cells to convey information about stimulus features independent of their response amplitude (Albrecht and Hamilton, 1982; Heeger, 1992). Our findings that spike threshold varies with stimulus orientation and instantaneous firing rate (data not shown) are consistent with this interpretation.

Another effect will be to dynamically regulate the sensitivity to coincident synaptic input. This is supported by our finding that the decrease in threshold that occurs with rapid depolarization depends inversely on the magnitude of sustained depolarization. Because the rate of V_m depolarization is proportional to the precision of synchronous excitatory inputs (Destexhe and Pare, 1999; Azouz and Gray, 2000), we interpret our findings as evidence for an adaptive coincidence-detection mechanism. Thus, during high-input states evoked by sensory stimulation, our findings predict that spike generation is driven preferentially by those excitatory inputs that are highly synchronous. Such effects could be further enhanced by transient synchronous inhibition (Whittington et al., 1995; Buzsaki and Chrobak, 1995). The hyperpolarization evoked by inhibitory inputs arriving immediately prior to excitation would further reduce spike threshold in response to the ensuing synchronous excitation. Interactions of this sort would tend to be self-reinforcing and favor the generation of high-frequency oscillations (Gray and Singer, 1989).

These conclusions mesh well with another experimental finding of this study. The orientation specificity of evoked γ band fluctuations (28–80 Hz) was closely correlated with the spike activity of the cells (Gray and Singer, 1989; Gray et al., 1990), while the $\overline{V}_{m,tm}$ and the low-frequency fluctuations were more broadly tuned (Nelson et al., 1994; Pei et al., 1994; Azouz et al., 1997; Volgushev et al., 2000; Carandini and Ferster, 2000; Anderson et al., 2000a). While previous studies have argued that orientation tuning is enhanced by a "tip of the iceberg" effect, in which spikes are generated only by those depolarizations that cross a fixed firing threshold (Carandini and Ferster, 2000; Anderson et al., 2000a), our results are inconsistent with this interpretation. Rather than invoking a static nonlinearity, defined by a fixed threshold, our results suggest that orientation tuning is sharpened by a cooperative process in which synchronous activity in the network is amplified by adaptive coincidence detection to generate spike output. In this framework, the broadening of orientation tuning, predicted by the linear dependence of threshold on V_m, would be offset by the nonlinear dependence of threshold on dV_m/dt. This conjecture is consistent with two sets of experimental findings: action potentials most commonly arise from brief depolarizations reflecting synchronous synaptic inputs (Azouz and Gray, 1999, 2000), and visually evoked neuronal firing rates depend not only on the magnitude of depolarization but also on the amplitude of the high-frequency V_m components (Azouz and Gray, 1999; Anderson et al., 2000a; Volgushev and Eysel, 2000). Thus, both discharge characteristics and response selectivity can be explained, in part,

Table 2. Parameters Used for the H-H Model Simulations

	Na^+	K^+
Equilibrium potential	$E_{Na+} = 50mV$	$E_{K+} = -90mV$
Peak conductance	10 ms cm^{-2}	11 mS cm^{-2}
α_m	$0.091(V_m + 40)/(1 - \exp(-(V_m + 40)/5))$	
β_m	$-0.062(V_m + 40)/(1 - \exp(-(V_m + 40)/5))$	
α_h	$0.06 \exp((-55 - V_m)/15)$	
β_h	$6.01 \exp((17 - V_m)/21) + 1$	
α_s	$0.001 \exp((-85 - V_m)/30)$	
β_s	$0.034 \exp((-17 - V_m)/10) + 1$	
α_n		$0.034(V_m + 45)/(1 - \exp(-(V_m)/5))$
β_n		$0.54 \exp(-75 - V_m)/40$

The Na^+ current was given by the equation $I_{Na} = G_{Na}m^3hs(V_m - E_{Na})$, where m, h, and s are the activation, inactivation, and slow inactivation variables, respectively. The K^+ current was given by the equation $I_K = G_K n^4(V_m - E_K)$, where n is the activation variable. The temperature coefficient (Q_{10}) was assumed to be 5.

by a dynamic spike-encoding mechanism that is predominantly sensitive to synchronous synaptic inputs.

Implications for High-Input Conditions

Several theories have postulated a fundamental role for neuronal synchronization in cortical function (Milner, 1974; von der Malsburg, 1981; Singer and Gray, 1995; Gray, 1999; Diesmann et al., 1999; Abeles, 1982). While these models remain to be rigorously tested, their underlying assumptions have been criticized on physiological grounds (Shadlen and Newsome, 1998; Shadlen and Movshon, 1999). The essence of this argument is that neuronal synchrony cannot be reliably detected under high-input conditions, because cortical neurons are incapable of distinguishing significant synchronous inputs from those that occur by chance. Our findings contradict this argument. They suggest that the spike-generating mechanism enhances the relative sensitivity to synchronous inputs under high-input conditions, even though the absolute sensitivity decreases. Because of technical limitations, it is not possible to directly test this prediction. However, another line of evidence supports our conclusions. Several recent studies have demonstrated that cellular input conductance, measured somatically in cortical neurons in vivo, increases by up to 4-fold during states of strong synaptic input (Pare et al., 1998; Borg-Graham et al., 1998; Hirsch et al., 1998; Anderson et al., 2000c). This has at least two predicted effects on the postsynaptic response to synaptic input. It decreases the amplitude and shortens the time course of the postsynaptic potential (Destexhe and Pare, 1999; for an experimental verification of this prediction, see D. Heck et al., 2000, Soc. Neurosci., abstract). Thus, synaptic input becomes less effective, and its window for temporal integration narrows. Under these conditions, only those excitatory inputs that are highly synchronized will evoke rapid depolarizations of the magnitude reported here and elsewhere using in vivo intracellular recording. The remaining inputs, if acting independently, will evoke sustained changes in V_m that serve to sharpen the sensitivity to synchronous inputs. Based on these considerations, we propose that adaptive changes in spike threshold act synergistically with changes in input conductance evoked by sensory stimulation to select and amplify synchronous activity in cortical networks.

Experimental Procedures

Experimental Methods

All experiments were conducted on anesthetized and paralyzed adult cats of both genders. The methods for induction and maintenance of anesthesia, surgical preparation, and intracellular recording in vivo have been described in detail in previous reports (Azouz and Gray, 1999, 2000). Quantitative data were obtained in response to a minimum of 20 presentations of a drifting sine wave or square wave grating (10–20 cd/m^2 mean luminance, 80 Hz noninterlaced refresh rate, 1024 × 768 resolution) presented to the dominant eye at the preferred orientation, direction, velocity, and spatial frequency. The data recorded on each trial consisted of a 0.5 s period of spontaneous activity followed by 2–3 s of visual stimulation and were digitized at a rate of 20 kHz. In some cells (n = 15), we also recorded the responses to a complete range of stimulus directions at intervals of 22.5°. All procedures followed guidelines established by the National Institutes of Health on the use of laboratory animals and were approved by the Institutional Animal Care and Use Committee.

Data Analysis

The aim of our analysis was to determine how spike threshold varies with V_m and its rate of change during the period immediately preceding a spike (dV_m/dt), and whether these threshold variations influence the discharge properties and feature selectivity of cortical cells. To accomplish these goals, we used a combination of data analysis and numerical simulations.

We divided the analysis of our experimental data into two parts. The first part consisted of data selection, calculation of the *baseline*-V_m, and measurement of spike thresholds. For data selection, we chose only those cells having a resting V_m of <-60mV, and action potentials that exceeded 0mV and did not decrease appreciably in amplitude (>10mV) during sustained depolarization. This served to exclude recordings of poor quality and putative dendritic impalements. For the selected cells, we calculated the *baseline*-V_m by taking the grand average of all the data points (excluding action potentials, see below) in the first 250 ms of spontaneous activity across all the trials in a session. This measure served as the approximate equivalent of the resting V_m for each cell in the absence of visual stimulation. We then normalized the data on each trial by subtracting the *baseline*-V_m from each data point during the visual response. This enabled us to express the results of our subsequent calculations relative to a putative resting V_m.

The methods for spike threshold detection have been described in detail in previous reports (Azouz and Gray, 1999, 2000). Briefly, we identified the voltage preceding each spike, which, once reached, resulted in an action potential. We computed the maximum rate of change of V_m $(dV_m/dt)_{max}$ over three consecutive data points during the upstroke of each spike and calculated dV_m/dt for each interval of time preceding the peak slope. Threshold was defined as the voltage at the onset of each spike at which dV_m/dt first reached an empirically determined fraction of $(dV_m/dt)_{max}$. This ratio (0.033) was chosen when the value of dV_m/dt resulted in a close match to the threshold assigned by careful visual inspection of the raw data.

In the second part, we examined the influence of V_m and dV_m/dt on spike threshold for the signals recorded immediately prior to each spike. To accomplish this, we first split the signal into its two components, subthreshold V_m fluctuations and spike activity. The spikes were truncated at their threshold voltages and their times of occurrence (i.e., leading edge) stored at 1 ms resolution. The truncated record of V_m was resampled at 1 kHz, and any remaining voltage transients were removed by applying a sliding three-point median filter. These calculations served to remove the spikes without affecting the underlying subthreshold V_m fluctuations.

To assess the influence of V_m on threshold, we computed the linear correlation between spike threshold and the average value of V_m (excluding spikes) over the 250 ms period preceding each spike. We use the symbol $\overline{V}_{m,ps}$ to denote this quantity, where the subscript *ps* stands for prespike. We chose a value of 250 ms because it gave an adequate estimate of the mean while keeping the influence of transient fluctuations to a minimum (we performed the same calculations using windows of 64 and 128 ms prior to each spike and found similar results [data not shown]). Similarly, to assess the influence of dV_m/dt, we calculated the mean rate of depolarization over the 10 ms period preceding each spike and fit the distribution relating this measure to the corresponding spike threshold using a monoexponential function ($Y = a + be^{-\dot{V}/\nu_t}$, where $\dot{V} = dV_m/dt$, and ν_t is the decay constant in units of mV/ms). We chose a value of 10 ms based on our calculations of the spike-triggered average of V_m, which revealed that the rising phase of the transient depolarization preceding a spike typically lasts 10–15 ms (Azouz and Gray, 1999). For this analysis, spikes were selected if they were separated by at least 20 ms from any preceding spike. This enabled us to exclude the influence of high firing rates on this measure (interspike intervals greater than 6 ms duration had no observable effect on spike threshold; data not shown). This calculation was performed on a trial-by-trial basis to exclude the influence of large changes in the spontaneous V_m that occur across trials (Destexhe and Pare, 1999; Azouz and Gray, 1999). Finally, to study the combined relation between V_m and dV_m/dt, we measured the linear correlation between the average V_m during the visual response on each trial ($\overline{V}_{m,tm}$) and the decay constants derived from the exponential fits. $\overline{V}_{m,tm}$ was computed from the baseline-subtracted subthreshold activity during the entire period of visual stimulation. The subscript *tm* denotes trial mean.

Throughout the manuscript, average values are reported as means ± 1 standard deviation.

Neuronal Simulations

In order to determine the influence of dynamic threshold on discharge properties and stimulus selectivity, we derived current waveforms from the continuous records of V_m evoked by visual stimulation (after removing the spikes). We then injected these currents into two types of single-compartment model neurons, one endowed with Hodgkin and Huxley (H-H)-like voltage-gated Na^+ and K^+ conductances and an otherwise identical integrate-and-fire (I&F) model neuron. Because this procedure is known to result in filtering of the original signals by the resistive and capacitive properties of the membrane (Nowak et al., 1997), we converted the V_m records to current according to the following formula:

$$I_{inject} = I_{Res} + I_{Cap} = V/R_{in} + (dV/dt)C_{in},$$

where I_{Res}, I_{Cap}, R_{in}, and C_{in} are resistive current, capacitive current, input impedance, and membrane capacitance, respectively. The values of R_{in} and C_{in} were estimated by the responses of the recorded cells to repetitive 0.1–0.2 nA hyperpolarizing current pulses in the absence of visual stimulation. The result of these simulations yielded two types of V_m records, one consisting of the responses of a passive model having a fixed threshold (the I&F model) and another obtained from an identical model capable of actively generating spikes (the H-H model). We then compared the mean firing rates of both model responses to identical sets of stimuli.

In order to determine the influence of active spike generation on orientation bandwidth, we repeated the analysis using responses to drifting bars over a 360° range of directions, at 22.5° intervals. We fit the resulting distributions relating firing rate as a function of direction to a Gaussian function and obtained an estimate of tuning bandwidth (2σ of Gaussian) for each measure.

We conducted the numerical simulations using NEURON (Hines, 1989) and modeled the cells as a single isopotential compartment (R_m = 125 KΩ cm^2, C_m = 1 μF/cm^2, and R_{in} = 30 MΩ, resting V_m = −70mV). Voltage-gated Na^+ and K^+ conductances were implemented using the Hodgkin-Huxley equations (Hodgkin and Huxley, 1952a, 1952b; Noble, 1966). The maximal conductances and the activation and inactivation variables were derived from experimental data (Huguenard et al., 1988; Hamill et al., 1991; Belluzzi and Sacchi, 1991; Fleidervish et al., 1996) and are given in Table 2. The spike threshold for the integrate-and-fire model (−55mV) was adjusted to correspond to the spike threshold level in a Hodgkin-Huxley model injected with a 5 ms depolarizing pulse at the resting V_m.

Acknowledgments

We thank Russ Himmelspach for his excellent care of the animals. Extensive discussions with Shih Cheng Yen, Michael Wehr, and John Miller greatly improved the manuscript. This work was supported by a grant to C.M.G. from the National Eye Institute.

Received: July 1, 2002
Revised: November 13, 2002

References

Abeles, M. (1982). Local Cortical Circuits: An Electrophysiological Study (Berlin: Springer).

Albrecht, D.G., and Hamilton, D.B. (1982). Striate cortex of monkey and cat: contrast response function. J. Neurophysiol *48*, 217–237.

Alonso, J.M., Usrey, W.M., and Reid, R.C. (1996). Precisely correlated firing in cells of the lateral geniculate nucleus. Nature *385*, 815–819.

Anderson, P., Storm, J., and Wheal, H.V. (1987). Thresholds of action potentials evoked by synapses on the dendrites of pyramidal cells in the rat hippocampus in vitro. J. Physiol. *383*, 509–526.

Anderson, J.S., Lampl, I., Gillespie, D.C., and Ferster, D. (2000a). The contribution of noise to contrast invariance of orientation tuning in cat visual cortex. Science *290*, 1968–1972.

Anderson, J.S., Lampl, I., Reichova, I., Carandini, M., and Ferster, D. (2000b). Stimulus dependence of two-state fluctuations of membrane potential in cat visual cortex. Nat. Neurosci. *3*, 617–621.

Anderson, J.S., Carandini, M., and Ferster, D. (2000c). Orientation tuning of input conductance, excitation, and inhibition in cat primary visual cortex. J. Neurophysiol. *84*, 909–926.

Azouz, R., and Gray, C.M. (1999). Cellular mechanisms contributing to response variability of cortical neurons *in vivo*. J. Neurosci. *19*, 2209–2223.

Azouz, R., and Gray, C.M. (2000). Dynamic spike threshold reveals a mechanism for synaptic coincidence detection in cortical neurons in vivo. Proc. Natl. Acad. Sci. USA *97*, 8110–8115.

Azouz, R., Gray, C.M., Nowak, L.G., and McCormick, D.A. (1997). Physiological properties of inhibitory interneurons in cat striate cortex. Cereb. Cortex *7*, 534–545.

Belluzzi, O., and Sacchi, O. (1991). A five-conductance model of the action potential in the rat sympathetic neurone. Prog. Biophys. Mol. Biol. *55*, 1–30.

Borg-Graham, L.J., Monier, C., and Fregnac, Y. (1998). Visual input evokes transient and strong shunting inhibition in visual cortical neurons. Nature *393*, 369–373.

Bringuier, V., Fregnac, Y., Baranyi, A., Debanne, D., and Shulz, D.E. (1996). Synaptic origin and stimulus dependency of neuronal oscillatory activity in the primary visual cortex of the cat. J. Physiol. *500*, 751–774.

Buzsaki, G., and Chrobak, J.J. (1995). Temporal structure in spatially organized neuronal ensembles: a role for interneuronal networks. Curr. Opin. Neurobiol. *4*, 504–510.

Cantrell, A.R., and Catterall, W.A. (2001). Neuromodulation of Na+ channels: an unexpected form of cellular plasticity. Nat. Rev. Neurosci. *2*, 397–407.

Carandini, M., and Ferster, D.A. (1997). Tonic hyperpolarization un-

derlying contrast adaptation in cat visual cortex. Science *276*, 949–952.

Carandini, M., and Ferster, D. (2000). Membrane potential and firing rate in cat primary visual cortex. J. Neurosci *20*, 470–484.

Carandini, M., Mechler, F., Leonard, C.S., and Movshon, J.A. (1996). Spike train encoding by regular-spiking cells of the visual cortex. J. Neurophysiol *76*, 3425–3441.

Carr, D.B., Cooper, D.C., Ulrich, S.L., Spruston, N., and Surmeier, D.J. (2002). Serotonin receptor activation inhibits sodium current and dendritic excitability in prefrontal cortex via a protein kinase C-dependent mechanism. J. Neurosci. *22*, 6846–6855.

Destexhe, A., and Pare, D. (1999). Impact of network activity on the integrative properties of neocortical pyramidal neurons *in vivo*. J. Neurophysiol. *81*, 1531–1547.

Diesmann, M., Gewaltig, M.O., and Aertsen, A. (1999). Stable propagation of synchronous spiking in cortical neural networks. Nature *402*, 529–533.

Fleidervish, I.A., Friedman, A., and Gutnick, M.J. (1996). Slow inactivation of Na^+ current and slow cumulative spike adaptation in mouse and guinea-pig neocortical neurones in slices. J. Physiol. *493*, 83–97.

Fricker, D., Verheugen, J.H.S., and Miles, R. (1999). Cell-attached measurements of firing threshold of rat hippocampal neurons. J. Physiol. *517*, 791–804.

Fries, P., Reynolds, J.H., Rorie, A.E., and Desimone, R. (2001). Modulation of oscillatory neuronal synchronization by selective visual attention. Science *291*, 1506–1507.

Gray, C.M. (1994). Synchronous oscillations in neuronal systems: mechanisms and functions. J. Comput. Neurosci. *1*, 11–38.

Gray, C.M. (1999). The temporal correlation hypothesis of visual feature integration: still alive and well. Neuron *24*, 31–47.

Gray, C.M., and McCormick, D.A. (1996). Chattering cells: superficial pyramidal neurons contributing to the generation of synchronous oscillations in visual cortex. Science *274*, 109–113.

Gray, C.M., and Singer, W. (1989). Stimulus-specific neuronal oscillations in orientation columns of cat visual cortex. Proc. Natl. Acad. Sci. USA *86*, 1698–1702.

Gray, C.M., Engel, A.K., Koenig, P., and Singer, W. (1990). Stimulus-dependent neuronal oscillations in cat visual cortex: Receptive field properties and feature dependence. Eur. J. Neurosci. *2*, 607–619.

Hamill, O.P., Huguenard, J.R., and Prince, D.A. (1991). Patch-clamp studies of voltage-gated currents in identified neurons of the rat cerebral cortex. Cereb. Cortex *1*, 48–61.

Heeger, D.J. (1992). Normalization of cell responses in cat striate cortex. Vis. Neurosci *9*, 181–198.

Henze, D.A., and Buzsaki, G. (2001). Action potential threshold of hippocampal pyramidal cells *in vivo* is increased by recent spiking activity. Neuroscience *105*, 121–130.

Hines, M.A. (1989). Program for simulation of nerve equations with branching geometries. Int. J. Biomed. Comput. *24*, 55–68.

Hirsch, J.A., Alonso, J.M., Reid, R.C., and Martinez, L.M. (1998). Synaptic integration in striate cortical simple cells. J. Neurosci. *18*, 9517–9528.

Hodgkin, A.L., and Huxley, A.F. (1952a). The dual effects of membrane potential on sodium conductance in giant axon of Loligo. J. Physiol. *116*, 497–506.

Hodgkin, A.L., and Huxley, A.F. (1952b). A quantitative description of membrane current and its application to conduction and excitation in nerve. J. Physiol. *117*, 500–544.

Huguenard, J.R., Hamill, O.P., and Prince, D.A. (1988). Developmental changes in Na^+ conductances in rat neocortical neurons: appearance of a slowly inactivating component. J. Neurophysiol. *59*, 778–795.

Jagadeesh, B., Gray, C.M., and Ferster, D. (1992). Visually-evoked oscillations of membrane potential in neurons of cat striate cortex studied with in vivo whole cell patch recording. Science *257*, 552–554.

Margulis, M., and Tang, C.-M. (1998). Temporal integration can readily switch between sublinear and supralinear summation. J. Neurophysiol. *79*, 2809–2813.

Milner, P. (1974). A model for visual shape recognition. Psychol. Rev *81*, 521–535.

Nelson, S., Toth, L., Sheth, B., and Sur, M. (1994). Orientation selectivity of cortical neurons during intracellular blockade of inhibition. Science *265*, 774–777.

Noble, D. (1966). Applications of Hodgkin-Huxley equations to excitable tissues. Physiol. Rev. *46*, 1–47.

Nowak, L.G., Sanchez-Vives, M.V., and McCormick, D.A. (1997). Influence of low and high frequency inputs on spike timing in visual cortical neurons. Cereb. Cortex *7*, 487–501.

Pare, D., Shink, E., Gaudreau, H., Destexhe, A., and Lang, E.J. (1998). Impact of spontaneous synaptic activity on the resting properties of cat neocortical pyramidal neurons in vivo. J. Neurophysiol. *79*, 1450–1460.

Pei, X., Vidyasagar, T.R., Volgushev, M., and Creutzfeldt, O.D. (1994). Receptive field analysis and orientation selectivity of postsynaptic potentials of simple cells in cat visual cortex. J. Neurosci. *14*, 7130–7140.

Schwindt, P.C., and Crill, W.E. (1995). Amplification of synaptic current by persistent sodium conductance in apical dendrite of neocortical neurons. J. Neurophysiol. *74*, 2220–2224.

Shadlen, M.N., and Movshon, J.A. (1999). Synchrony unbound: a critical evaluation of the temporal binding hypothesis. Neuron *24*, 67–77.

Shadlen, M.N., and Newsome, W.T. (1998). The variable discharge of cortical neurons: implications for connectivity, computation and information coding. J. Neurosci. *18*, 3870–3896.

Singer, W., and Gray, C.M. (1995). Visual feature integration and the temporal correlation hypothesis. Annu. Rev. Neurosci. *18*, 555–586.

Steinmetz, P.N., Roy, A., Fitzgerald, P.J., Hsiao, S.S., Johnson, K.O., and Niebur, E. (2000). Attention modulates synchronized neuronal firing in primate somatosensory cortex. Nature *404*, 187–190.

Stuart, G., and Sakmann, B. (1995). Amplification of EPSPs by axosomatic sodium channels in neocortical pyramidal neurons. Neuron *15*, 1065–1076.

Usrey, W.M., and Reid, R.C. (1999). Synchronous activity in the visual system. Annu. Rev. Physiol. *61*, 435–456.

Volgushev, M., and Eysel, U.T. (2000). Noise makes sense in neuronal computing. Science *290*, 1908–1909.

Volgushev, M., Pernberg, J., and Eysel, U.T. (2000). Comparison of the selectivity of postsynaptic potentials and spike responses in cat visual cortex. Eur. J. Neurosci. *12*, 257–263.

von der Malsburg, C. (1981). The Correlation Theory of Brain Function. Internal Report, Max-Planck-Institute for Biophysical Chemistry, Gottingen, West Germany.

Whittington, M.A., Traub, R.D., and Jefferys, J.G. (1995). Synchronized oscillations in interneuron networks driven by metabotropic glutamate receptor activation. Nature *373*, 612–615.